

## Functions of long non-coding RNA LNC11649 in non-small cell lung cancer cells as a reprocessed form of MALAT1

Jun-Zhe QI<sup>1</sup>, Ting-Ting ZHAO<sup>2</sup>, Shu-Shan QI<sup>2\*</sup>

<sup>1</sup>Department of Clinical Medicine, Chongqing Medical University, Chongqing, China; <sup>2</sup>Department of Thoracic Surgery, Liangxiang Hospital of Beijing Fangshan District, Beijing, China

\*Correspondence: shushanqi@aliyun.com

Received July 5, 2022 / Accepted October 18, 2022

Long non-coding RNAs (lncRNAs) have received much attention concerning their expression mechanisms in tumor formation. It is known that lncRNAs are involved in the occurrence, development, and prognosis of various tumors, including lung cancer. In our study, one non-coding RNA, LNC11649 (649 nt in length), was identified in non-small cell lung cancer (NSCLC) by PacBio third-generation sequencing technology. Both northern blot and quantitative PCR analyses confirmed the presence of LNC11649 in NSCLC tissues and cells with high expression. Its sequence was found to be highly homologous to lncRNA MALAT1. Knocking down MALAT1 could lead to a significant downregulation of LNC11649 content, revealing the possibility that LNC11649 could originate from MALAT1 reprocessing. RNA immunoprecipitation and electrophoretic mobility shift assays confirmed an interaction between LNC11649 and the MSI1 protein. Further experiments revealed that LNC11649 promoted the cytoplasmic distribution of MSI1 through its interaction with MSI1 and then activated the Akt signaling pathway to regulate the proliferation and migration of NSCLC cells. Our study reveals the possibility that LNC11649 plays a cancer-promoting role as a reprocessed form of MALAT1 in NSCLC cells and suggests that the MALAT1/LNC11649/MSI1/Akt regulatory axis becomes a potential therapeutic target for lung cancer.

*Key words:* lncRNA, non-small cell lung cancer, MALAT1, LNC11649, MSI1

Lung cancer ranks first in morbidity and mortality among malignant tumors and constitutes the leading cause of cancer-related deaths globally [1, 2]. Based on histopathology, lung cancer can be divided into two major types: small cell lung cancer and non-small cell lung cancer (NSCLC). Due to the lack of specific clinical symptoms in the early stage of lung cancer, lung cancer diagnosis usually occurs in the late stage, and the 5-year survival rate for these patients is only 16–18%. The biological process of the occurrence and evolution of lung cancer is regulated by many factors. Understanding lung cancer related regulatory factors and exploring the molecular mechanism of this cancer is of great significance in providing early detection, diagnosis, and treatment of lung cancer. Long non-coding RNAs (lncRNA) are a class of RNA molecules with transcripts longer than 200 nucleotides with established cell or tissue specificity [3]. lncRNAs have been confirmed to play regulatory roles in gene expression at epigenetic, transcriptional, and post-transcriptional levels. It has been documented that lncRNAs can participate in various cytological processes, including chromatin modifi-

cation, regulation of gene expression, and cell differentiation [4]. They can also affect tumor metastasis and invasion, tumor cell proliferation, apoptosis, and tumor angiogenesis, regulate tumor drug resistance, and promote or inhibit the occurrence and development of lung cancer, providing a new strategy for the treatment of lung cancer [5, 6]. In addition, lncRNAs can also be used as potential biomarkers for early diagnosis and disease prognosis of multiple malignant tumors, including lung cancer [7].

Metastasis-associated lung adenocarcinoma transcript 1 (MALAT1) is one of the most widely studied nuclear-restricted lncRNAs and has generated much attention in recent years due to its abundance, rather ubiquitous expression, and apparent role in various disease manifestations. MALAT1, also known as nuclear-enriched abundant transcript 2, was first identified during microarray screening of tumors in patients with NSCLC and was found to be upregulated in tumors with a high propensity for metastasis [8]. Since this initial study, overexpression of this lncRNA has been reported in more than 20 solid tumors or lymphomas. Its high level of expression has been linked to

tumor progression and metastasis [8–12]. Elevated expression levels of MALAT1 have been shown to be associated with poor prognosis in various solid and hematopoietic cancers [13–15]. In addition, the overexpression of MALAT1 has been associated with metastasis in lung, breast, and liver cancers [9, 16, 17]. In mouse models of metastatic cancer, MALAT1 deletion or knockdown resulted in a significant reduction in differentiation and metastasis of the primary tumor [9]. Furthermore, in a lung cancer homing model, both the knockdown and knockout of MALAT1 reduced the homing of lung cancer cells to the lung [18]. Similar observations have been reported in colorectal, esophageal, gallbladder, cervical, and prostate cancers, where MALAT1 knockdown abrogated tumor growth and/or metastasis in the respective cell line-derived or PDX mouse models [19–21]. In many of these studies, MALAT1 knockdown affected the transcription or pre-mRNA splicing of key genes involved in migration and cell adhesion.

The MALAT1 gene is localized on human chromosome 11q13.1 and mouse chromosome 19qA. It is located in a gene-dense region with very high synthetic evolutionary conservation [22]. MALAT1 exhibits significant sequence conservation, with overall >50% conservation in vertebrates and >80% at the 3' end of the transcript [23]. This is one of the main features of MALAT1, as few lncRNAs show such a high level of evolutionary conservation. The primary transcript of MALAT1 is processed into the well-characterized nuclear conserved MALAT1 transcript and produces a small tRNA-like RNA from its 3' end [24]. Post-processing of the nuclear retained MALAT1 transcript results in no polyadenylation at the 3' end; however, it contains a genomically encoded poly(A)-rich extension that pairs with an upstream U-rich region and then adopts a unique triple-helical structure [25, 26]. This triple-helical structure has been shown to confer MALAT1 stability and nuclear localization in the absence of a true poly(A) tail. Despite the relative stability afforded to MALAT1 by the triple-helical structure, however, human MALAT1 is approximately 8,700 nt long, and maintaining an intact structure at such a length is theoretically quite challenging. Indeed, there is evidence for the existence of different spliceosomes of MALAT1 beyond its full length [27]. Ageeli et al. also observed that specific triplex-disruptive mutations lead to the degradation of MALAT1 and a loss of nuclear accumulation [28]. These studies suggest the possibility of the existence of other short fragments of the conserved MALAT1 splice with a complex expression pattern of transcriptional variants.

The latest generation of sequencing technology, PacBio, is a single-molecule real-time sequencing technology developed by Pacific Bioscience in the USA [29], with no requirement for PCR amplification in the sequencing process. Compared with second-generation sequencing techniques, PacBio offers advantages such as much longer read lengths than those obtained with second-generation methods and no GC preference, which can significantly improve genome

assembly quality. Furthermore, the most significant advantage of PacBio in the study of transcriptomics is that it can obtain full-length or near full-length transcripts, which is of great significance for the identification of alternative splicing [30, 31], the analysis of lncRNA [32], and the discovery of new genes [30]. In addition, it can supplement and even lead to the discovery of new mechanisms based on the original research.

We attempted to explore the possibility of the existence of MALAT1 transcript variants by RNA sequencing in NSCLC tissues and corresponding paracancerous tissues using PacBio sequencing technology. In this study, we selected one of the sequences with the highest number of reads and proposed to perform a preliminary exploration of the functional mechanism in NSCLC cells.

## Patients and methods

**Tissue samples.** The collected tissue samples were obtained from patients who underwent thoracic surgery at the Department of Oncology, Liangxiang Hospital of Beijing Fangshan District, from January 2018 to March 2019. Samples were separated and quickly placed in liquid nitrogen, then transported and stored in a refrigerator at  $-80^{\circ}\text{C}$ . The inclusion criteria for patients were adenocarcinoma or squamous cell carcinoma, absence of multiple primary tumors, absence of preoperative antitumor therapy, clear TNM stage, and complete clinical records. The clinic characteristics of the 21 patients are listed in Supplementary Table S1. The study was approved by the Clinical Research Ethics Committee of Liangxiang Hospital of Beijing Fangshan District (approval no. Jinglianglun-PD201652), and written informed consent was obtained from each participant in the study.

**Data source and processing.** The RNA expression data (level 3) were downloaded from TCGA data portal (<https://portal.gdc.cancer.gov/>). RNA-seq data (lncRNA and mRNA) from 108 non-tumor tissues and 1,037 non-small cell lung cancer tissues were included. The RNAseq data in FPKM (Fragments Per Kilobase Per Million) format is converted into LOG2. Statistical analysis and visualization were performed using R (version 3.6.3). This study was conducted in accordance with the publication guidelines provided by TCGA (<http://cancergenome.nih.gov/publications/publicationguidelines>).

The cellular localization of lncRNA was defined based primarily on the Locate-R subcellular localization database (<http://locate-r.azurewebsites.net/>) [33]. Online RBPmap (<http://rbpmap.technion.ac.il/index.html>) and catRAPID ([http://service.tartagialab.com/page/catrapid\\_group](http://service.tartagialab.com/page/catrapid_group)) were used to determine potential binding proteins for LNC11649 [34, 35].

**Sequencing analysis.** Tissue RNA was extracted by TRIzol (Thermo Fisher Scientific, Inc., MA, USA). According to the manufacturer's instructions, 4  $\mu\text{g}$  mixed RNA and PacBio

Sequel systems (Pacific Biosciences, CA, USA) were used for full-length transcriptional sequence sequencing. Using Clontech Smarter PCR cDNA synthesis kit and Pacific Biosciences luePippin Size Selection system (PN100-092800-03), the Iso-Seq library was prepared according to the isomer sequencing (Iso-Seq) protocol. Genex Health Co., Ltd. (Beijing, China) completed the follow-up sequencing and analysis.

**Cell culture and transfection.** Human NSCLC cell lines A549 (SCSP-503), H2170 (SCSP-602), HCC827 (SCSP-538), and SW900 (SCSP-53153) were purchased from the Center for Basic Medical Cells, Peking Union Medical College. The human normal bronchial epithelial cell line (BEAS-2B, cat. no. CL-0496) was purchased from Shanghai YiYan Biotechnology Co., Ltd. (Shanghai, China). MALAT1 knockout cell line H2170 was purchased from Ubigene (Guangdong, China). All cell lines were maintained in RPMI-1640 medium supplemented with 10% fetal bovine serum (FBS; Thermo Fisher Scientific), 2 mM glutamine (Gibco, Waltham, MA, USA), and 1% penicillin/streptomycin (Gibco) at 37°C with 5% CO<sub>2</sub>. MK2206 (2 μM) was purchased from Selleck (Selleck Chemicals, Shanghai, China) and was used to treat indicated groups of cells in culture.

Cell transfection was performed with Lipofectamine 3000 reagent (Thermo Fisher Scientific). Transfections were performed with siRNAs (10 nM) or plasmids (10 ng/μl) in 24-well or 96-well pretreated culture plates according to the manufacturer's recommendations. The lentiviral vectors of LNC11649 wild type (LV6-LNC11649) and mutant (LV6-LNC11649-mut) were constructed by GenePharma (Shanghai GenePharma Co., Ltd, China). NC siRNA: 5'-UUGUACUACACAAAAGUACUG-3'; MALAT1 siRNA: 5'-GGAAAGTAAAGCCCTGAACTA-3'; LNC11649 siRNA: 5'-GGGAGTGGTAGGATGAAACAA-3'; MSI1 siRNA: 5'-GGTGACTCGAACGAAGAAGAT-3'. All siRNAs were designed and synthesized by GenePharma (GenePharma Co., Ltd., Shanghai, China).

**Quantitative real-time polymerase chain reaction (qRT-PCR).** Total RNA was extracted with TRIzol reagent (Thermo Fisher Scientific). RNA concentration was quantified by spectrophotometry at 260 nm (Nanodrop, Wilmington, DE, USA). cDNA was generated by reverse transcription with the PrimeScript™ RT kit (TaKaRa Bio Inc., Shiga, Japan). The mixture was incubated at 37°C for 60 min, followed by incubation at 95°C for 5 min. Real-time PCR was performed using TB Green® Premix Ex Taq™ (TaKaRa) and ABI 7500 Real-Time PCR System (Applied Biosystems, Warrington, UK). The data were processed using the 2<sup>-ΔΔCT</sup> method [36]. GAPDH was used as an endogenous control.

Primer sequences are listed below: GAPDH forward, 5'-GGAGCGAGATCCCTCCAAAAT-3'; GAPDH reverse, 5'-GGCTGTTGTCATACTTCTCATGG-3'; LNC11649 forward, 5'-CATGACGCAGGGAGAATTGC-3'; LNC11649 reverse, 5'-GCCTTCCCGTACTTCTGTCTT-3'; MALAT1 forward, 5'-GTCATAACCAGCCTGGCAGT-3'; MALAT1

reverse, 5'-CGAAACATTGGCACACAGCA-3'; MSI1 forward, 5'-AATACTTCGGCCAGTTCGGG-3'; MSI1 reverse, 5'-AGTCACCATCTTGGGCTGTG-3';

**RNA fluorescence *in situ* hybridization.** For RNA FISH, cells were fixed in 4% paraformaldehyde (Sigma-Aldrich) for 10 min at room temperature. Cells were then washed twice with PBS and then fixed and permeabilized with 100% methanol for 10 min at room temperature. Methanol was aspirated, and the hybridization probes (10 ng) in RNA FISH buffer (2× SSC, 10% formamide, and 10% dextran sulfate) were added directly to the cells. MALAT1 and LNC11649 were detected using FITC or Cy3-labeled DNA probe complementary to the template (RiboBio, Guangzhou, China). The hybridization probes used in RNA FISH experiments are a mixture of multiple oligonucleotide probes of 20–50 nt length against the target [37]. The probes were incubated with the cell samples overnight in a humidified chamber at 37°C. The samples were then washed 6 times with 2×SSC. Hoechst 33342 (Thermo Fisher Scientific, 5 μg/ml) was used to label cell nuclei. Finally, cells were mounted in ProLong® Gold anti-fading reagent and observed with a fluorescence microscope (IX71, Olympus, Japan).

**Western blot analysis.** Cell lysates were prepared using Cell Lysis Buffer (Cell Signaling) containing a protease inhibitor cocktail. The same amount of sample protein (50 μg) was loaded on an SDS-PAGE gel. Firstly, the sample was electrophoresed and transferred to PVDF membranes (Bio-Rad, Hercules, CA, USA). Secondly, the membrane was blocked with 3% skim milk (Yili Company, Chifeng, China) in PBS at room temperature for 2 h, and incubated with the following primary antibodies at 4°C overnight. The bound antibody was detected by a horseradish peroxidase-labeled secondary antibody, and an enhanced chemiluminescence substrate was used (Thermo Fisher Scientific). The positive signal of the target protein was observed by Tanon 2500 image analyzer (Shanghai, China). The primary antibodies for MSI1 (ab52865, 1:1000), Lamin B1 (ab16048, 1:1000), Akt (ab8805, 1:1000), p-Akt (phospho T308, ab38449, 1:1000), and GAPDH (ab9485, 1:1000) were purchased from Abcam (Cambridge, UK). HRP-coupled goat anti-rabbit secondary antibody (#98164, 1:5000 dilution) was from Cell Signaling Technology (Beverly, MA, USA).

**Immunofluorescence.** 4% formaldehyde was used to fix the cells for 10 min. After washing, the cells were rehydrated with 4% BSA (BSA-PBS) solution at room temperature and blocked for 1 hour. Then, MSI1 primary antibody (ab52865, Abcam, 1:250) diluted in 4% BSA (BSA-PBS) was added and incubated for 1 h at room temperature. After washing in PBS, the secondary antibody was incubated with Alexa Fluor 488-labeled secondary antibody diluted in 4% BSA (BSA-PBS) for 1 h at room temperature, then washed in PBS, and mounted on a coverslip with ProLong Gold with 4'-6-diamidino-2-phenylindole (DAPI, Thermo Fisher Scientific, 1 mg/ml). Images were captured using a fluorescence microscope (IX71, Olympus, Japan).

**Cell viability assay.** Cell proliferation was detected by CCK-8 and EdU assays. CCK-8 assay was used to detect the cell proliferation rate. In short,  $4 \times 10^3$  transfected cells/well were re-seeded into 96-well plates and incubated for 1, 2, 3, and 4 d, respectively. Ten  $\mu\text{l}$  of CCK-8 reagent (Dojindo, Japan) was added to each well and incubated for 2 h. Then, a multimode reader (PerkinElmer, USA) was used to verify the OD450 nm value of each well. EdU assay was performed using an EdU assay kit (RiboBio). The cells were seeded in 96-well plates and treated with transfection for 24 hours. Then, 50  $\mu\text{M}$  EdU was added into the culture medium. After incubation at 37°C for 2 h, the cells were fixed with 4% paraformaldehyde. According to the standard procedure, cells were incubated with an anti-EdU working solution and DAPI for 30 min. The experimental results were observed under a fluorescence microscope (IX71, Olympus, Japan) and randomly recorded in different visual fields.

**Migration and invasion assay.** Cell migration was evaluated by Transwell assay using Transwell chambers (8  $\mu\text{m}$  pore size; Corning, NY, USA). Briefly, the treated cells of each group were inoculated into the upper chamber with a serum-free medium according to the number of  $3 \times 10^4$  cells, and 800  $\mu\text{l}$  medium containing 20% fetal bovine serum was added to the lower chamber. After continuous culture for 24 h, the small chamber was taken out and washed three times with PBS. The remaining cells were fixed with methanol for 15 min, stained with crystal violet, observed under a fluorescence microscope, and photographed in more than 5 visual fields randomly. Invasion assays were conducted similarly. The cell invasion assay was also similar except that 50  $\mu\text{l}$  of Matrigel (Sigma-Aldrich) diluted 1:8 in a serum-free medium was added to each well overnight before seeding the cells on the membrane.

**Electrophoretic mobility shift assay (EMSA).** Purified recombinant MSI1 protein was purchased from Sino Biological (Sino Biological Inc., Beijing, China). Biotin-labeled RNA probes (LNC11649-WT and LNC11649-MUT) were transcribed *in vitro* with biotin RNA labeling mix (Roche, St. Louis, MO, USA) and T7 RNA polymerase (Promega, Madison, WI, USA) according to manufacturer's instructions. LNC11649-mut has a "UAGAA" deletion mutation at 218-222 nt. EMSA was performed using the LightShift chemiluminescence EMSA kit (Thermo Fisher Scientific) as recommended by the manufacturer. In the presence or absence of the unlabeled probes (1 pmol), the labeled probe (20 fmol) was incubated with the MSI1 protein (200 ng) in a binding buffer for 30 min. All EMSA tests were performed on 5% polyacrylamide gel in Tris/borate/EDTA buffer (45 mM Tris-borate and 1 mM EDTA, Sigma-Aldrich). EMSA gels were electro-blotted onto Hybond-N+ membranes (GE Healthcare, Chicago, IL, USA). Membranes were exposed to Tanon 2500 image analyzer with a CCD camera (Tanon, Shanghai, China) for luminescence detection.

**Northern blot.** Northern blotting was performed using the North2South™ Chemiluminescent Hybridization and Detec-

tion Kit (Thermo Fisher Scientific). A total of 10  $\mu\text{g}$  of RNA from the indicated cells was subjected to formaldehyde gel electrophoresis and transferred to Hybond-N+ membranes (GE Healthcare). Biotin-labeled cDNA probes complementary to the template were obtained from RiboBio (Guangzhou, China). After prehybridization for 60 min, hybridization was continued for 12 h at 68°C in a hybridization buffer containing denatured probes. After washing according to the protocol, hybridization results were detected using a Tanon 2500 image analyzer (Tanon, Shanghai, China).

**RNA immunoprecipitation.** pEXP-LNC11649 plasmids were transfected into A549 cells using Lipofectamine 3000. Forty-eight hours later, RNA immunoprecipitation (RIP) experiments were conducted with the Magna RIP™ RNA-Binding Protein Immunoprecipitation Kit (Millipore, Bedford, MA, USA), and the primary antibodies (2  $\mu\text{g}$ ) or immunoglobulin G [IgG] control with protein G magnetic beads. After washing, RNAs bound to proteins were eluted and subjected to qRT-PCR analysis (see qRT-PCR protocol). RNA fold enrichment to input was calculated and normalized to IgG. The primary antibodies for HNRNPA1 (sc-32301), HNRNPA2B1 (sc-374053), MSI1 (sc-135721, 1:1000), and SRSF9 (sc-293314) were purchased from Santa Cruz Biotechnology (Santa Cruz, CA, USA), and the antibodies for PABPN1 (ab75855) and TRA2A (ab138448) were from Abcam (Cambridge, UK).

**Cycloheximide chase assay.** Cycloheximide chase assay was performed as previously described [38]. In brief, cells were treated with cycloheximide (20  $\mu\text{g}/\text{ml}$ ) for the indicated time periods (0, 2, 4, 6, and 8 h). Following treatment, cells were harvested at specific times, washed in PBS, and lysed in lysis buffer (150 mM NaCl, 50 mM Tris (pH 7.5), 0.5% NP-40, and protease inhibitors (Sigma-Aldrich)). BCA Protein Assay kit (Thermo Fisher Scientific) was used to measure protein concentration. Western blot was performed as described earlier.

**RNA stability assay.** Groups of cells were treated with 5  $\mu\text{M}$  actinomycin D (Sigma-Aldrich) to inhibit the transcription of mRNA. Cells were collected at 0, 4, 8, and 12 h post-treatment, and total RNA was extracted and used for qRT-PCR.

**Xenograft tumor models.** All mouse experiments were entrusted to Beijing Viewsolid Biotech Co., Ltd. with animal ethics approval number VS212601441. A549 cell line with stable expression of LNC11649 was obtained by screening with G418 (500  $\mu\text{g}/\text{ml}$ , Sigma-Aldrich, St. Louis, MO, USA) in the selective medium under pressure for 4 weeks. A549 cells ( $2 \times 10^6$ ) were subcutaneously inoculated into one side of the back of the non-obese diabetic-severe combined immunodeficiency (NOD-SCID) mice. The following animal humane endpoints were established: tumors exceeding 10% of mice's body weight, tumors that festered or became infected, and mice who could not eat or drink on their own. The tumor models were euthanized when they reached experimental or humane endpoints. 2.5 l of CO<sub>2</sub> was used for 5–7 minutes to euthanize the mice. After four weeks, the tumors were

harvested, and tumor masses were measured and weighed. The tumor volume was calculated according to the formula: Tumor volume =  $0.5236 \times (\text{length} \times \text{width}^2)$ . All animal experiments were approved by the Laboratory Animal Ethics Committee of Beijing Viewsolid Biotech Co., Ltd. (approval no. VS212601441). Animal procedures followed the guidelines issued by the China Animal Protection Association.

**Statistical analysis.** Statistical analyses were performed using GraphPad Prism 7.0 (GraphPad Software). Data are presented as means  $\pm$  standard deviation (SD). Sets containing two groups of data are analyzed using double-tailed Student's t-test or Mann-Whitney U test. The sets with more than two groups of data were analyzed by one-way ANOVA with Dunnett post hoc analysis or two-way ANOVA with Tukey post-hoc analysis. If the p-value  $<0.05$ , the difference is considered to be statistically significant.

## Results

**Abnormally high expression of lncRNA LNC11649 in NSCLC tissues and cells.** Using PacBio sequencing analysis in lung cancer and corresponding adjacent tissues, a previously unreported high-abundance lncRNA with the highest number of reads (240 reads) (Figure 1A, Supplementary Table S2,) was identified in our preliminary analysis. It is 649 nt in length and was temporarily named LNC11649. According to quantitative PCR analysis in the collected 21 pairs of NSCLC tissues and corresponding adjacent tissues, abnormally high expression of LNC11649 was verified in lung cancer tissues (Figure 1B). A subsequent comparative analysis was performed concerning the expression of LNC11649 in normal lung epithelial cells (BEAS-2B) and various NSCLC cells (A549, HCC827, H2170, and SW900). Consistently, as observed in tissues, the relative content of LNC11649 in lung cancer cells was significantly higher than that found in BEAS-2B cells (Figure 1C). In addition, when all group comparisons were made, it did not yield the conclusion that the level of LNC11649 was significantly higher in lung squamous carcinoma cells than in lung adenocarcinoma cells, e.g., HCC827 vs. SW900 ( $p=0.3371$ ). Similarly, in lung cancer tissues ( $n=21$ ), containing 6 cases of lung squamous carcinoma and 15 cases of lung adenocarcinoma, the conclusion that LNC11649 was higher in lung squamous carcinoma tissues than in lung adenocarcinoma was not obtained.

**Correlation between LNC11649 and lncRNA MALAT1.** Subsequent analyses demonstrated that LNC11649 was located on chromosome 11 (65499045-65499693) and that lncRNA MALAT1 was also located on chromosome 11 (65497738-65506512), suggesting that LNC11649 might only be a degradation fragment of lncRNA MALAT1. LNC11649 was further detected in lung cancer tissues using Northern blot analysis. It was found that a probe designed for LNC11649 could detect bands of 700 and approximately 7,000 nt (Figures 2A, 2B), while the length of mature MALAT1 was approximately 7,000 nt in length. Next, the

expression of MALAT1 was knocked down using siRNA in lung cancer H2170 cells (Figure 2C). Both quantitative PCR and northern blot results demonstrated that LNC11649 was significantly downregulated along with the downregulation of MALAT1 expression (Figures 2D, 2E). In the MALAT1 knockout cell line H2170, the overexpression of wild-type MALAT1 resulted in a strong detection signal for LNC11649. However, overexpression of mutant MALAT1 (deletion of a 649 nt nucleic acid fragment) was not effective in detecting the presence of LNC11649 (Figures 2F, 2G). These results suggest that LNC11649 with a length of 649 nt might originate from MALAT1. Restated, LNC11649 might be a short fragment of MALAT1.

Notably, MALAT1 was initially found to be upregulated in NSCLC with a high propensity for metastasis [8], but overall, there was no abnormal differential expression in NSCLC tissues compared to normal tissues based on TCGA database (Figure 2H). Similarly, intact MALAT1 expression was not significantly different in A549, HCC827, H2170, and SW900 cells compared with BEAS-2B cells (Figure 2I). However, LNC11649, as a short segment of MALAT1, is highly expressed in lung cancer tissues and cells (Figures 1B, 1C), which seems to be more tumor-specific than MALAT1.

**LNC11649 has biological functions in lung cancer cells.** With reference to the above findings, was LNC11649 only a degradation product of MALAT1 or a functional

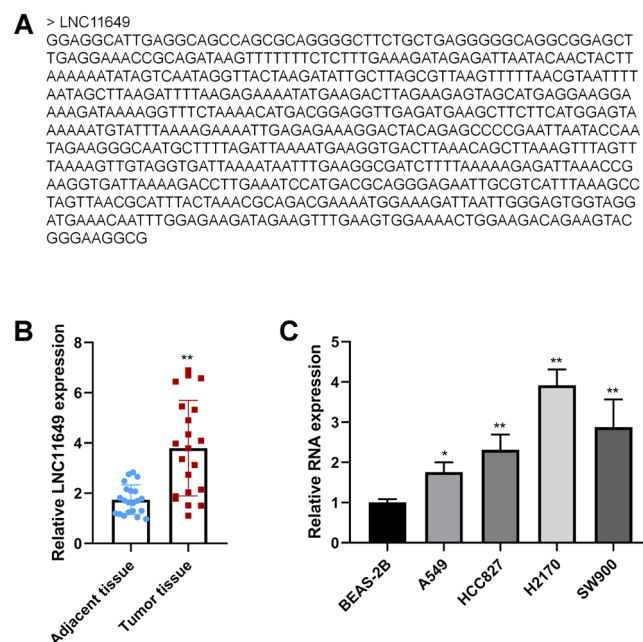


**Figure 1. Expression characteristics of LNC1164 in tissues and NSCLC cells.** A) Sequence for LNC1164 obtained by PacBio sequencing analysis. B) Expression of LNC1164 in lung cancer and adjacent tissues using quantitative PCR. Compared with adjacent tissue,  $n=21$ , paired Student's t-test,  $**p<0.01$ . C) Expression of LNC1164 in NSCLC cells and normal lung epithelial cells using quantitative PCR. One-way ANOVA with Dunnett post hoc analysis. Compared with BEAS-2B cells,  $*p<0.05$ ;  $**p<0.01$ .

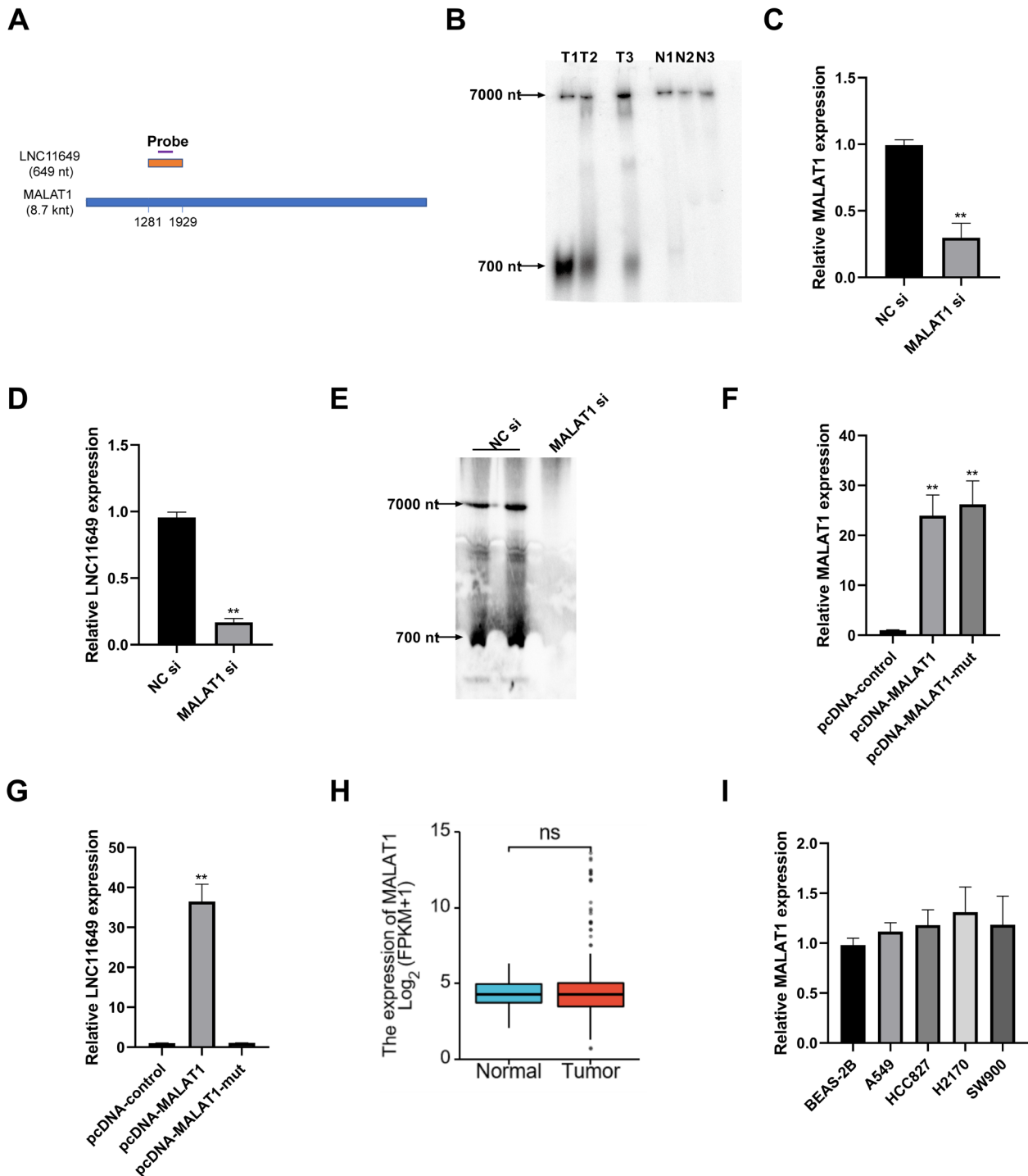


Figure 2. Correlation analysis between LNC11649 and lncRNA MALAT1. A) Schematic of the correlation between LNC11649 and lncRNA MALAT1 sequences and the design of hybridization probes based on the sequences. B) Relative expression of LNC11649 in lung cancer tissues and corresponding adjacent tissues was demonstrated using northern blot analysis. T1-3 refers to tumor tissues, and N1-3 refers to normal corresponding adjacent tissues. C) Silencing effect of siRNA on MALAT1 in H2170 cells was demonstrated using quantitative PCR. Compared with the NC-si group,  $**p < 0.01$ . D) Relative content of LNC11649 after MALAT1 knockdown by siRNA in H2170 cells demonstrated by quantitative PCR. Compared with the NC-si group,  $**p < 0.01$ . E) Relative content of LNC11649 after MALAT1 knockdown by siRNA in H2170 cells was demonstrated using northern blot analysis. F, G) Overexpression of wild-type or mutant MALAT1 in MALAT1 knockout cell lines and detection of the relative expression levels of MALAT1 and LNC11649 using quantitative PCR. H) Relative expression of the MALAT1 gene in different NSCLC samples and normal control tissues based on TCGA database. I) Relative expression of the MALAT1 gene in various NSCLC cells and normal lung epithelial cells was demonstrated using quantitative PCR. One-way ANOVA with Dunnett post hoc analysis (F, G, and I).  $**p < 0.01$

RNA fragment in lung cancer cells? Online Locate-R (<http://locate-r.azurewebsites.net/>) was then used for the sequence analysis, and the corresponding prediction results revealed that LNC11649 could be located in the cytoplasm (Figure 3A). Subsequently, cytoplasmic/nuclear RNA extraction and quantitative PCR results demonstrated that MALAT1 was localized in the nucleus, while LNC11649 was distributed abundantly in the cytoplasmic region (Figure 3B). In addition, the results of RNA-FISH experiments in H2170 cells produced similar results (Figure 3C).

We attempted to overexpress LNC11649 in A549 and HCC827 cells that contain lower amounts of LNC11649 (Figure 4A, Supplementary Figure S1A). The proliferation (Figures 4B–4D, Supplementary Figures S1B–S1D), migration, and invasion ability of lung cancer cells were

significantly upregulated (Figures 4E, 4F; Supplementary Figures S1E, S1F) along with an increase in LNC11649 content. Further, to assess the *in vivo* effects of LNC11649, we constructed a mouse model of xenograft tumors using A549 cells that were transfected stably with LNC11649. Tumor volumes and weights were significantly higher in the LNC11649 group than in the control group (Figures 4G–4I). These experimental results suggest that LNC11649 is biologically functional and contributes to the malignant phenotype of NSCLC cells.

**Interaction between LNC11649 and RNA-binding proteins (RBPs).** To further understand the biological function of LNC11649, we attempted to determine the proteins with which it interacts. Online RBPmap (<http://rbpmap.technion.ac.il/index.html>) and catRAPID ([\*\*A SUBCELLULAR LOCALIZATION\*\*

Ribosome  
Nucleus  
Exosome  
Cytoplasm

\*\*B\*\*

Relative MALAT1 abundance

Relative LNC11649 abundance

Nucleus  
Cytoplasm

GAPDH U1 MALAT1

GAPDH U1 LNC11649

\*\*C\*\*

Probe Hoechst Merge

MALAT1

LNC11649](http://</a></p>
</div>
<div data-bbox=)

**Figure 3.** Subcellular localization analysis of LNC11649. A) Prediction of cell localization of LNC11649 by Locate-R. B) Quantitative PCR analysis of the subcellular location of MALAT1 and LNC11649 in H2170 cells. GAPDH and U1 snRNA were used as a cytoplasm and nuclear localization marker, respectively. C) *In situ* hybridization analysis of the subcellular location of MALAT1 and LNC11649 in H2170 cells. Green: FITC-labeled; red: Cy3-labeled; blue: Hoechst 33342. Scale bar=20  $\mu$ m.

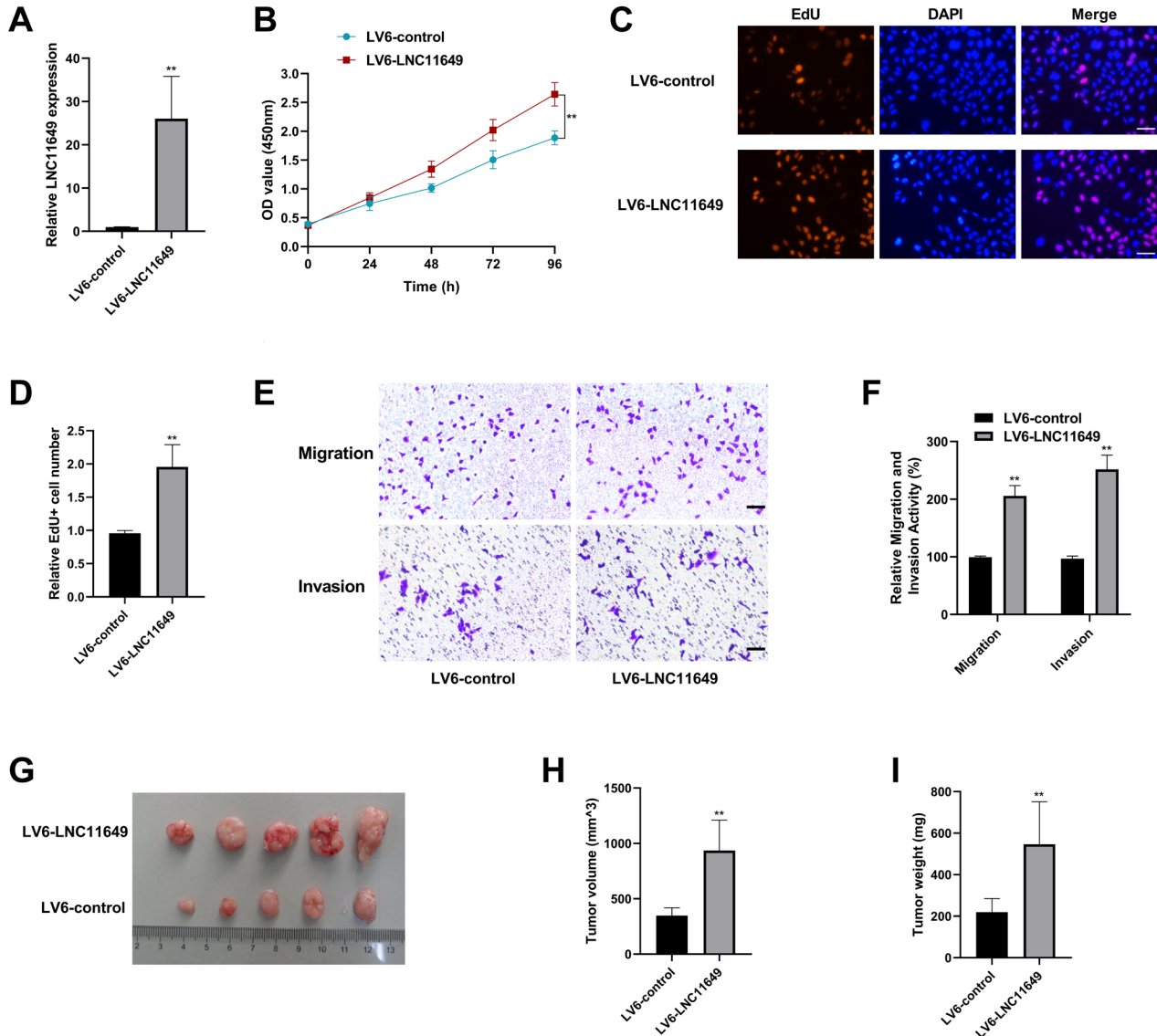


**Figure 4.** Functional analysis of LNC11649. **A**) A549 cells were transfected with a lentiviral control vector (LV6-control) or an LNC11649 lentiviral vector (LV6-LNC11649) for 48 h. Quantitative PCR was performed to detect the relative contents of LNC11649. \*\* $p < 0.01$  **B**) Detection of cell activity at different time points by CCK-8 after transfection with LNC11649 expression plasmid or control plasmid (1  $\mu\text{g}/\text{well}$  in the 24-well plate) in A549 cells. \*\* $p < 0.01$ , compared with the LV6-control group. **C, D**) Detection of cell proliferation by EdU staining after transfection with LNC11649 expression plasmid or control plasmid in A549 cells for 24 h (Scale bar=50  $\mu\text{m}$ ). Compared with the LV6-control group, \*\* $p < 0.01$  **E, F**) Detection of cell migration and invasion by Transwell assays after transfection with LNC11649 expression plasmid or control plasmid in A549 cells for 24 h (Scale bar=50  $\mu\text{m}$ ). Compared with the LV6-control group, \*\* $p < 0.01$  **G**) Representative images of tumor-bearing mice and images of xenograft tumors in each group are shown (n=5). **H**) Tumor volumes and **I**) weights were measured for both groups. Unpaired Student's t-test, \*\* $p < 0.01$

service.tartagliab.com/page/catrapid\_group) were used to determine potential binding proteins for LNC11649, and nine candidate proteins were identified (ANKHD1, G3BP2, HNRNPA1, HNRNPA2B1, MSI1, PABPN1, RBM3, SRSF9, and TRA2A) (Supplementary Table S3). Then, the online GEPIA tool (<http://gepia.cancer-pku.cn/>) was used to extract lung cancer-related data from TCGA database to analyze the expression differences of the candidate proteins. Conse-

quently, six proteins, including HNRNPA1, HNRNPA2B1, MSI1, PABPN1, SRSF9, and TRA2A, showed significantly higher relative expression levels in NSCLC tissue than in normal tissue (Figure 5A). Subsequently, due to the overexpression of LNC11649 in A549 cells, an RNA-IP experiment was performed using specific antibodies against candidate proteins. The results revealed that the MSI1 antibody significantly enriched LNC11649 (Figure 5B) but failed to effec-

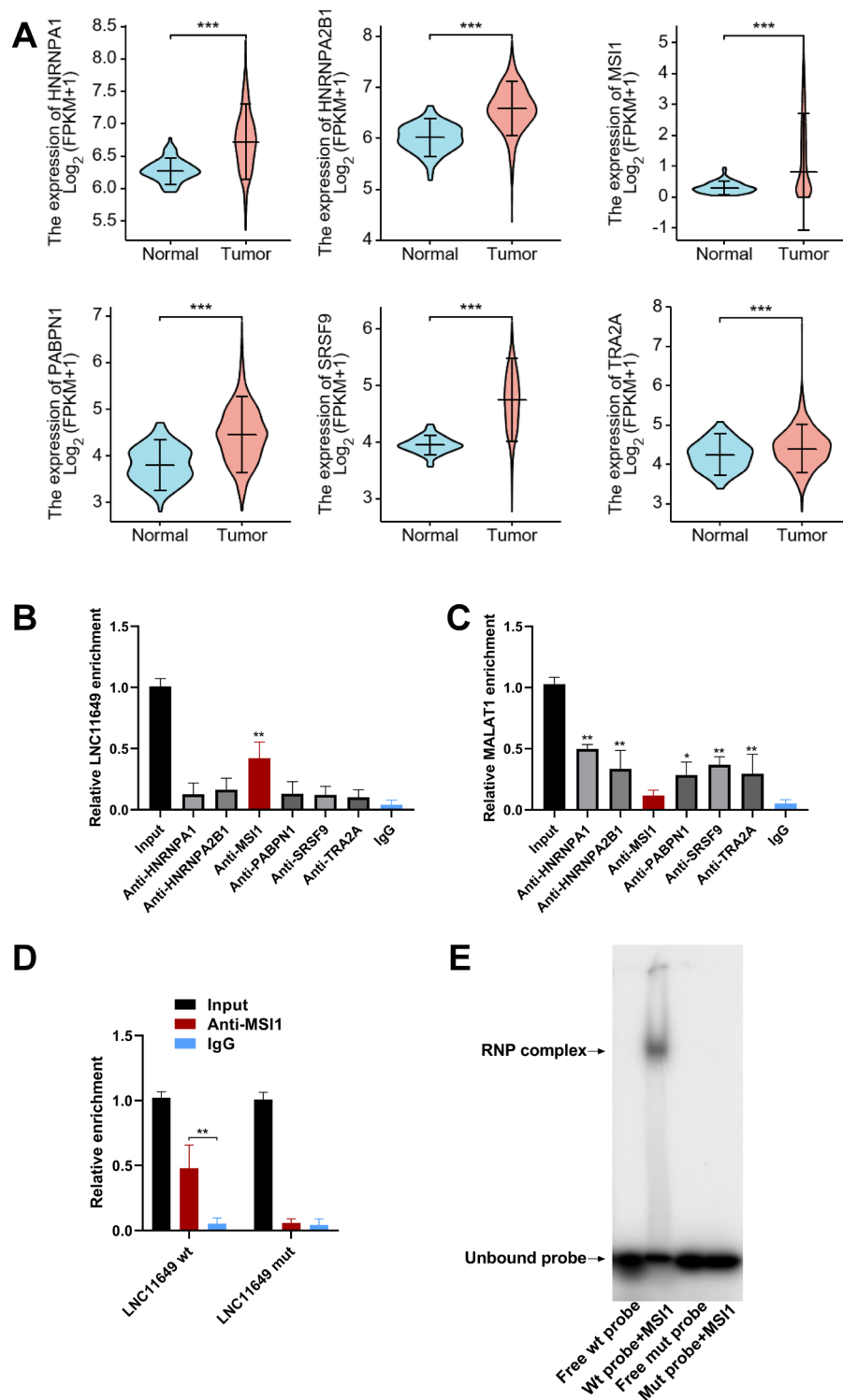
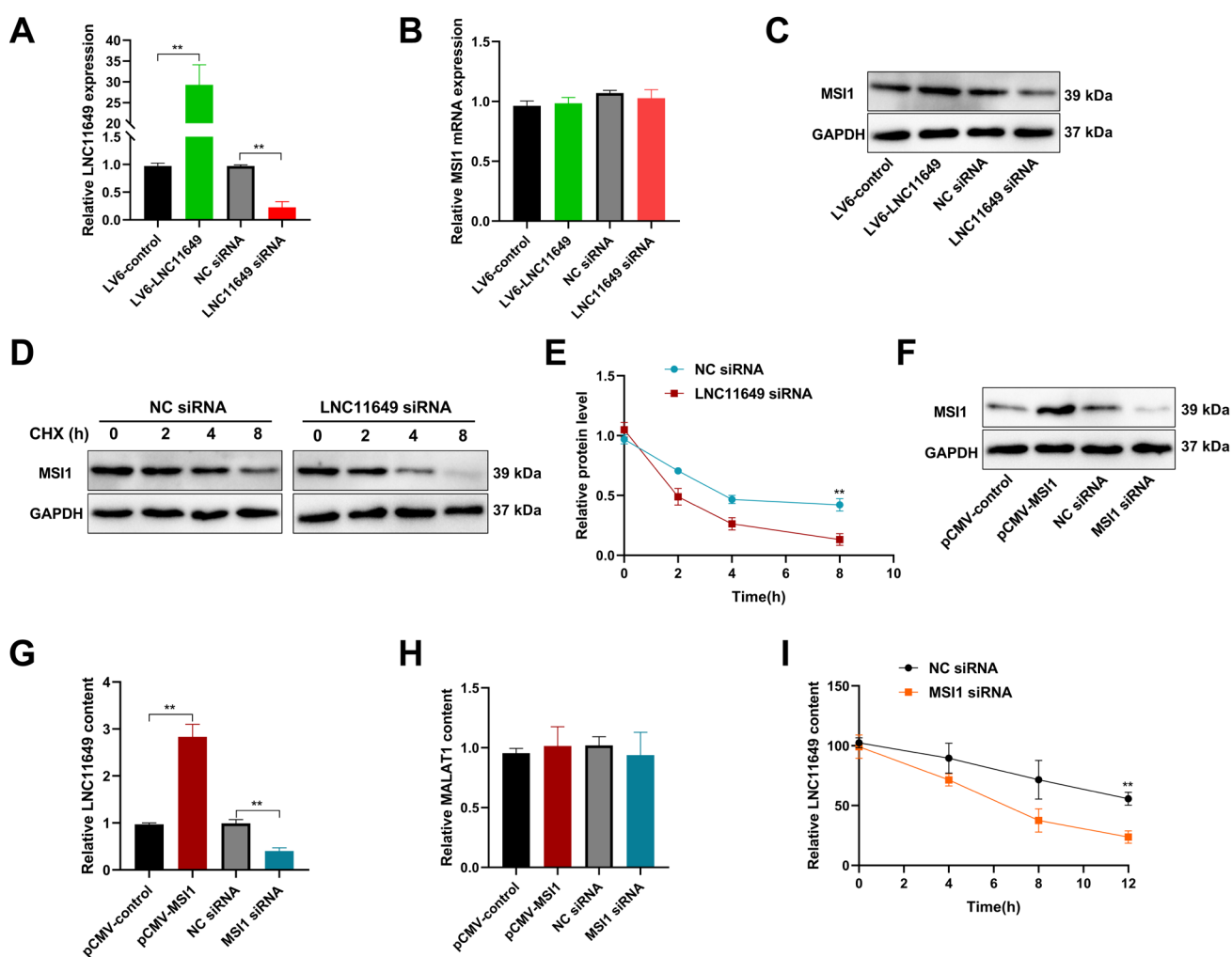


Figure 5. Identification of RNA-binding proteins (RBPs) that interact with LNC11649. A) Analysis of the relative expression levels of predicted genes that potentially interact with LNC11649 in different NSCLC samples and normal control tissues based on TCGA database analyses. Data: RNAseq data in level 3 HTSeq-FPKM format from TCGA (<https://portal.gdc.cancer.gov/>) Lung Adenocarcinoma/Lung Squamous Carcinoma (LUAD/LUSC) project. Compared with normal control tissues, \*\*\* $p < 0.001$ . B) RNA-IP experiments with specific antibodies against potential RBPs and detection of the enrichment of LNC11649 by quantitative PCR. \*\* $p < 0.01$ , compared with IgG. C) RNA-IP assays were performed for MALAT1. \* $p < 0.05$  and \*\* $p < 0.01$ , compared with IgG. D) Comparison of the enrichment of MSI1 antibody to wild-type and LNC11649-mut using quantitative PCR. Compared with IgG, \*\* $p < 0.01$ . E) Interaction of MSI1 protein with wild-type and LNC11649-mut using EMSA *in vitro*. One-way ANOVA with Dunnett post hoc analysis (B, C, and D), \*\* $p < 0.01$ .

tively enrich MALAT1 (Figure 5C). LNC11649-mut was constructed after deletion mutation at the MSI1 binding site (uagaa). The enrichment abundance of LNC11649-mut precipitated with MSI1 antibody was significantly lower than that of LNC11649-wt (Figure 5D). In addition, the results of electrophoretic mobility shift assay experiments with human recombinant MSI1 protein indicated that MSI1 could bind to LNC11649-wt but not LNC11649-mut (Figure 5E).

**The interaction of LNC11649 with MSI1 affects the stability of each.** Overexpression or knockdown of LNC11649

(Fig. 6A) in A549 cells did not affect the relative content of MSI1 mRNA (Figure 6B) but significantly altered the relative content of the MSI1 protein (Figure 6C), suggesting a possible post-transcriptional regulation of MSI1 expression by LNC11649. Cycloheximide chase assays were performed to characterize the stability of the MSI1 protein in A549 cells. The results indicate that the knockdown of LNC11649 significantly reduced the stability of the MSI1 protein (Figures 6D, 6E). Alternatively, when MSI1 was overexpressed in A549 cells (Figure 6F), the relative amount of LNC11649 was



**Figure 6.** The interaction of LNC11649 with MSI1 affects the stability of each. A) A549 cells were transfected with LNC11649 lentiviral vector (LV6-LNC11649) or LNC11649 siRNA for 48 h. Quantitative PCR was performed to detect the relative content of LNC11649. \*\* $p < 0.01$  B) After transfection with an LV6-LNC11649 vector or with LNC11649 siRNA in A549 cells for 48 h, the relative amounts of MSI1 were detected using quantitative PCR. C) After transfection with an LV6-LNC11649 vector or with LNC11649 siRNA in A549 cells for 48 h, the relative amount of MSI1 protein was detected by western blot analysis. D) After transfection with an LV6-LNC11649 vector or with LNC11649 siRNA in A549 cells for 24 h, MSI1 protein stability was assessed using a cycloheximide (CHX) chase assay. The cells were treated with CHX (20  $\mu\text{g}/\text{ml}$ ), and western blot analysis was performed using 50  $\mu\text{g}$  of cell lysates. E) At each time point, the density of the MSI1 protein bands was normalized to the density of the corresponding GAPDH bands. The level of remaining MSI1 protein at each time point was calculated as a ratio relative to the initial MSI1 protein level. \*\* $p < 0.01$  F) After transfection with an MSI1 overexpression vector (pCMV-MSI1) or with MSI1 siRNA in A549 cells for 48 h, the relative amount of MSI1 protein was detected by western blot analysis. G, H) After transfection with an MSI1 overexpression vector (pCMV-MSI1) or with MSI1 siRNA in A549 cells for 48 h, the relative amounts of LNC11649 and MALAT1 were detected by qPCR. \*\* $p < 0.01$  I) A549 cells were transfected with NC siRNA or with MSI1 siRNA for 24 h and continued to be treated with actinomycin D. At different time points, the relative content of LNC11649 was analyzed using quantitative PCR. One-way ANOVA with Dunnett post hoc analysis (A, B, G, and H), and two-way ANOVA with Tukey post-hoc analysis (E, I), \*\* $p < 0.01$

significantly upregulated (Figure 6G). Conversely, the knock-down of MSI1 (Figure 6F) decreased the relative content of LNC11649 (Figure 6F). However, either overexpression or knockdown of MSI1 did not significantly change the relative content of MALAT1 (Figure 6H), suggesting that MSI1 is not involved in regulating the initial transcript level of LNC11649. Next, quantitative PCR analysis was used to examine the stability of LNC11649 after RNA transcription was inhibited using actinomycin D in A549 cells. The results indicate that the knockdown of MSI1 resulted in a significant downregulation of the stability of LNC11649 (Figure 6I). The above experimental results demonstrate that interaction between LNC11649 and MSI1 favors the stability of each.

**Activation of the Akt signaling pathway by LNC11649 through interaction with MSI1.** Interestingly, we found that LNC11649 can be involved in regulating the cellular localization of MSI1. MSI1 was mainly located in the nucleus in A549 cells (Figures 7A, 7B), which, however, began to show an increasing trend of distribution in the cytoplasm with an increase in the LNC11649 content (Figures 7A, 7B), while no similar effect was observed following the overexpression of LNC11649-mut. Lang et al. reported that overexpression of MSI1 could activate the Akt pathway in NSCLC cells [39]. In our study, the phosphorylation level of Akt was found to be significantly upregulated with an increase in the cytoplasmic distribution of MSI1 (Figure 7C), which, however, exhibited no obvious change with the overexpression of LNC11649-mut. Furthermore, an increase in cell proliferation and migration induced by the overexpression of LNC11649-wt could be effectively inhibited by the Akt inhibitor MK2206 (Figures 7D–7F). As suggested by the aforementioned results, LNC11649 could change the cell localization of MSI1 through its interaction with MSI1 and then activate the Akt signaling pathway (Figure 8), thus promoting the malignant phenotypic characteristics of NSCLC cells.

## Discussion

Human MALAT1 is approximately 8,700 nt long. The primary transcription product, MALAT1, can form a tRNA-like clover-leaf secondary structure at hundreds of bases upstream of its polyadenylic acid site, which can be specifically recognized and bound by RNase P. It is then spliced at its upstream end to form two fragments: MALAT1 mature transcript with a size of 7,072 nt and a more minor transcript near the 3' end. The latter transcript is then transported to the cytoplasm and processed by RNase Z splicing. The CCA-adding enzyme adds CCA to its 3' end, which can form a mature tRNA-like transcript with a size of 61 nt and enter the cytoplasm [25, 40]. At present, MALAT1 is considered to be a highly stable lncRNA. Despite the absence of a poly-A tail at the 3' end of its mature transcript, it can produce a unique triple-helical structure. Such structures can play a protective role at the 3' end of MALAT1 against splicing by exonucleases [41]. In our study, the LNC11649 sequence was

detected using third-generation sequencing technology that originated from MALAT1, with confirmation of the actual existence of LNC11649 by northern blot analysis, revealing the possibility of MALAT1 being reprocessed. MALAT1 is also characterized by a high level of expression, which can be equivalent to highly transcribed housekeeping genes even in normal tissues, such as  $\beta$ -actin [22]. In view of the results of the analysis of gene expression data for lung cancer in TCGA database, there was no significant difference in MALAT1 expression between lung cancer and normal tissues. Furthermore, no apparent differences were observed in the transcripts of MALAT1 between several NSCLC cells and normal lung epithelial cells, while overexpression of LNC11649 was detected in lung cancer tissues and cells.

Since its discovery, MALAT1 appears to be upregulated only in tumors with a higher propensity to metastasize, including NSCLC [8–12]. The overall expression of MALAT1 in NSCLC (both high and low metastasis) in TCGA database is demonstrated in Figure 2H in the manuscript. The high expression of LNC11649 RNA in NSCLC is not directly derived from the difference in the expression content of MALAT1 but from the difference in its reprocessing in tumor and normal tissues. We performed parallel experiments in cancerous and corresponding paracancerous tissues. Both quantitative PCR and northern blot results showed that LNC11649 was present in cancer tissues at a high level (Figures 2B, 2C). The results of multiple samples and multiple experiments were able to illustrate the specificity of the presence of LNC11649 in tumor tissues. These results reveal that LNC11649, as a reprocessed product of MALAT1, has lung cancer cell specificity and selectivity. Unfortunately, there is a lack of understanding of the processing process at present.

In addition to affecting splicing and transcription, MALAT1 has also been reported to act as a ceRNA (competing endogenous RNA) or miRNA sponge to inhibit miRNAs and participate in miRNA network regulation under various conditions [42]. However, most miRNAs are enriched and functional in the cytoplasm [43]. To date, no studies have confirmed that intact MALAT1 has the ability to shuttle between the nucleus and the cytoplasm. How can MALAT1, located in the nucleus, inhibit the function of cytoplasmic miRNA is a contradictory and debatable problem. MALAT1 is a classic lncRNA with nuclear localization, while LNC11649 is localized in the cytoplasm. We initially predicted that LNC11649 would be capable of interacting with dozens of miRNAs, including miR-150-5p and miR-145-5p (Supplementary Table S4), which have typical oncogenic effects in NSCLC [44–47]. In our study, although interactions of LNC11649 with the predicted miR-150-5p and miR-145-5p were not identified in our preliminary research, the possibility of LNC11649 interacting with other miRNAs could not be excluded directly at this stage. In addition, it also remains to be clarified with respect to the possibility that MALAT1 may be reprocessed into other

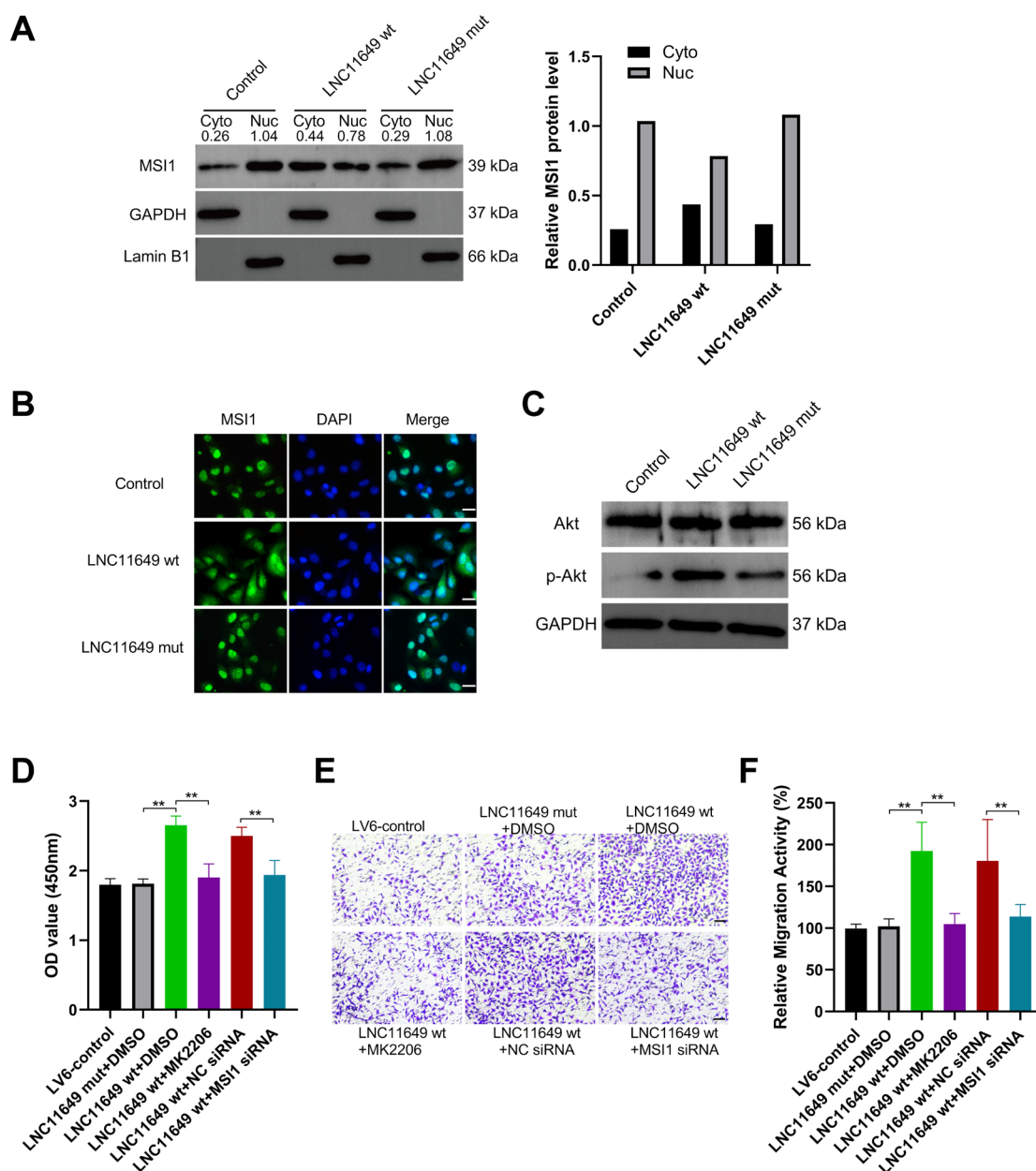


**Figure 7.** Activation of the Akt signaling pathway by LNC11649 through interaction with MSI1. **A**) Comparison of the distribution of MSI1 in the cytoplasm and nucleus by western blot analysis following the extraction of the cytoplasmic and nuclear proteins, respectively, after overexpression of wild-type or LNC11649-mut in A549 cells for 24 h. GAPDH and Lamin B1 were used as reference proteins for the cytoplasm and nucleus, respectively. The gray values were analyzed with ImageJ software. The bar chart compares the expression of relative gray values. **B**) Subcellular localization of MSI1 by immunofluorescence analysis after overexpression of wild-type or LNC11649-mut in A549 cells for 24 h. Magnification, 200 $\times$ ; Scale bar=20  $\mu$ m. **C**) The relative contents of Akt and phosphorylated Akt in cells in each group using western blot analysis after overexpression of the wild-type or LNC11649-mut in A549 cells for 24 h. **D**) Detection of cell activity in each group using the CCK-8 assay at different time points after the transfection of A549 cells with an LNC11649 expression plasmid and Akt inhibitor MK2206 (1.5  $\mu$ M) for 24 h. Compared with LNC11649-wt, \*\* $p$ <0.01. **E, F**) Detection of cell migration in each group by Transwell assays after the transfection of A549 cells with the LNC11649 expression plasmid and Akt inhibitor MK2206 (1.5  $\mu$ M) for 24 h. Magnification, 200 $\times$ ; Scale bar=50  $\mu$ m. Compared with LNC11649-wt, \*\* $p$ <0.01. One-way ANOVA with Dunnett post hoc analysis (**D, F**).

lncRNA sequences to be a ceRNA that can be localized to the cytoplasm. These hypotheses may partially address the current confusion that MALAT1 participates in competitive inhibition with miRNA.

The Musashi (MSI) family is an evolutionarily conserved group of RBPs that includes two members of Musashi-1 (MSI1) and Musashi-2 (MSI2) [48]. MSI1 is mainly expressed in the embryonic kidney, brain, liver, and lung and in the

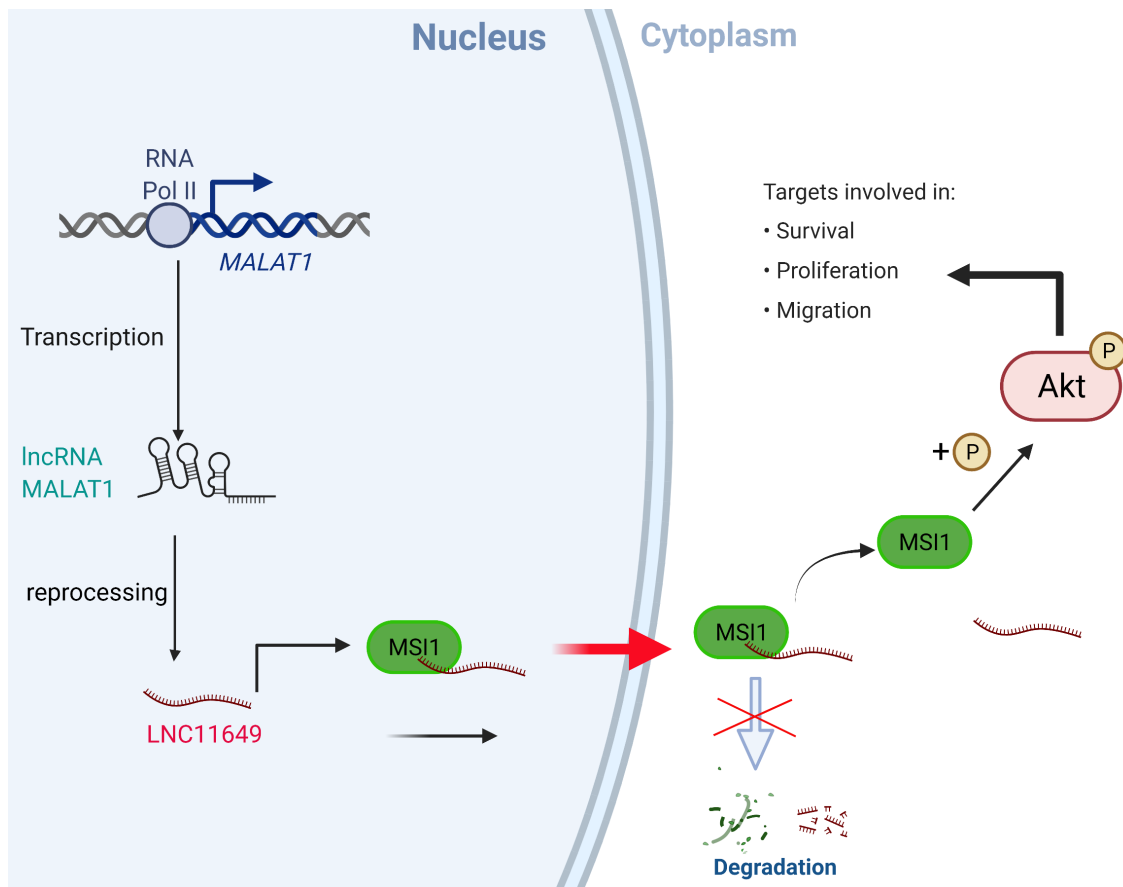


**Figure 8.** A diagram showing that LNC11649 changes the cellular localization of MSI1 and activates the Akt signaling pathway through its interaction with MSI1.

adult brain, pancreas, breast, and small intestine. MSI1 has been recognized to be a stem cell marker that mediates a balance between cell self-renewal and differentiation. Simultaneously, it is also involved in tumorigenesis and has been identified to be highly expressed in various tumor types such as gastric cancer, esophageal cancer, cervical cancer, colorectal cancer, and glioblastoma [48–50]. Furthermore, it has been reported that MSI1 can be used as a therapeutic target and diagnostic marker for lung cancer [51]. As an RBP, MSI1 has been shown to regulate the translation activity of many target genes related to tumor development, including Numb and Notch signaling pathways. For example, Lang et al. reported that the overexpression of MSI1 in NSCLC cells can promote Akt phosphorylation and activate the Akt signaling pathway [39]. Our experiments further demonstrated that the Akt signaling pathway could be activated more effectively and significantly when MSI1 interacted with LNC11649 and tended toward cytoplasmic localization. The interaction of RNA with proteins depends not only on the ribonucleotide sequence of RNA but also on the structures of RNA. Our experimental results showed that MSI1 was able to bind LNC11649 but did not interact with MALAT1, presum-

ably because the complex high-level structure of MALAT1 obscured the nucleic acid binding sites of MSI1 or hindered MSI1 binding in terms of spatial structure. So far, it is unclear to us that the high expression of LNC11649 leads to the dominant cytoplasmic localization of MSI1. It is unknown whether LNC11649 interacts with MSI1 in the cytoplasm first, limiting the nuclear translocation of MSI1, or whether LNC11649 binds preferentially to MSI1 in the nucleus before directing the cytoplasmic translocation of MSI1. The exact mechanism requires further in-depth exploration.

Furthermore, although our experimental results demonstrate the presence and function of the MALAT1/LNC11649/MSI1/Akt regulatory axis in NSCLC, the status of this regulatory axis in other cancer types is unknown to us so far, especially the newly discovered phenomenon of LNC11649 as a secondary processing product of MALAT1. The generalizability of LNC11649 in other cancers needs to be further verified in detail.

In conclusion, LNC11649, obtained from PacBio sequencing analysis, may originate from the reprocessing of lncRNA MALAT1. This result provides new insights into the stability of MALAT1, i.e., the stability of MALAT1 is

relative, and LNC11649 generated by secondary processing is not “waste” but functional. Furthermore, our studies confirm that LNC11649 can interact with MSI1 to activate the Akt signaling pathway and thus regulate the proliferation and migration of lung cancer cells. Our findings reveal the possibility that LNC11649 functions as a reprocessed form of MALAT1 that have a role in tumor promotion in NSCLC cells. Finally, the MALAT1/LNC11649/MSI1/Akt regulatory axis could become a potential therapeutic target for lung cancer.

**Supplementary information** is available in the online version of the paper.

**Acknowledgments:** This work is supported by the Scientific Research Subject of Liangxiang Hospital (Grant no. 2017-02).

## References

- [1] BRAY F, FERLAY J, SOERJOMATARAM I, SIEGEL RL, TORRE LA et al. Global cancer statistics 2018: GLOBOCAN estimates of incidence and mortality worldwide for 36 cancers in 185 countries. *CA Cancer J Clin* 2018; 68: 394–424. <https://doi.org/10.3322/caac.21492>
- [2] CAO W, CHEN HD, YU YW, LI N, CHEN WQ. Changing profiles of cancer burden worldwide and in China: a secondary analysis of the global cancer statistics 2020. *Chin Med J (Engl)* 2021; 134: 783–791. <https://doi.org/10.1097/CM9.0000000000001474>
- [3] RANSOHOFF JD, WEI Y, KHAVARI PA. The functions and unique features of long intergenic non-coding RNA. *Nat Rev Mol Cell Biol* 2018; 19: 143–157. <https://doi.org/10.1038/nrm.2017.104>
- [4] STATELLO L, GUO CJ, CHEN LL, HUARTE M. Gene regulation by long non-coding RNAs and its biological functions. *Nat Rev Mol Cell Biol* 2021; 22: 96–118. <https://doi.org/10.1038/s41580-020-00315-9>
- [5] BACH DH, LEE SK. Long noncoding RNAs in cancer cells. *Cancer Lett* 2018; 419: 152–166. <https://doi.org/10.1016/j.canlet.2018.01.053>
- [6] LIN YH. Crosstalk of lncRNA and Cellular Metabolism and Their Regulatory Mechanism in Cancer. *Int J Mol Sci* 2020; 21. <https://doi.org/10.3390/ijms21082947>
- [7] CHEN Y, ZITELLO E, GUO R, DENG Y. The function of lncRNAs and their role in the prediction, diagnosis, and prognosis of lung cancer. *Clin Transl Med* 2021; 11: e367. <https://doi.org/10.1002/ctm2.367>
- [8] JI P, DIEDERICH S, WANG W, BÖING S, METZGER R et al. MALAT-1, a novel noncoding RNA, and thymosin beta4 predict metastasis and survival in early-stage non-small cell lung cancer. *Oncogene* 2003; 22: 8031–8041. <https://doi.org/10.1038/sj.onc.1206928>
- [9] ARUN G, DIERMEIER S, AKERMAN M, CHANG KC, WILKINSON JE et al. Differentiation of mammary tumors and reduction in metastasis upon Malat1 lncRNA loss. *Genes Dev* 2016; 30: 34–51. <https://doi.org/10.1101/gad.270959.115>
- [10] AMODIO N, STAMATO MA, JULI G, MORELLI E, FULCINITI M et al. Drugging the lncRNA MALAT1 via LNA gapmeR ASO inhibits gene expression of proteasome subunits and triggers anti-multiple myeloma activity. *Leukemia* 2018; 32: 1948–1957. <https://doi.org/10.1038/s41375-018-0067-3>
- [11] OKUGAWA Y, TOIYAMA Y, HUR K, TODEN S, SAIGUSA S et al. Metastasis-associated long non-coding RNA drives gastric cancer development and promotes peritoneal metastasis. *Carcinogenesis* 2014; 35: 2731–2739. <https://doi.org/10.1093/carcin/bgu200>
- [12] AMODIO N, RAIMONDI L, JULI G, STAMATO MA, CARACCILOLO D et al. MALAT1: a druggable long non-coding RNA for targeted anti-cancer approaches. *J Hematol Oncol* 2018; 11: 63. <https://doi.org/10.1186/s13045-018-0606-4>
- [13] SCHMIDT LH, SPIEKER T, KOSCHMIEDER S, SCHÄFFERS S, HUMBERG J et al. The long noncoding MALAT-1 RNA indicates a poor prognosis in non-small cell lung cancer and induces migration and tumor growth. *J Thorac Oncol* 2011; 6: 1984–1992. <https://doi.org/10.1097/JTO.0b013e3182307eac>
- [14] VOCE DJ, BERNAL GM, WU L, CRAWLEY CD, ZHANG W et al. Temozolomide Treatment Induces lncRNA MALAT1 in an NF-κB and p53 Codependent Manner in Glioblastoma. *Cancer Res* 2019; 79: 2536–2548. <https://doi.org/10.1158/0008-5472.CAN-18-2170>
- [15] CHING T, PEPLAWSKA K, HUANG S, ZHU X, SHEN Y et al. Pan-Cancer Analyses Reveal Long Intergenic Non-Coding RNAs Relevant to Tumor Diagnosis, Subtyping and Prognosis. *EBioMedicine* 2016; 7: 62–72. <https://doi.org/10.1016/j.ebiom.2016.03.023>
- [16] MALAKAR P, SHILO A, MOGILEVSKY A, STEIN I, PIKARSKY E et al. Long Noncoding RNA MALAT1 Promotes Hepatocellular Carcinoma Development by SRSF1 Upregulation and mTOR Activation. *Cancer Res* 2017; 77: 1155–1167. <https://doi.org/10.1158/0008-5472.CAN-16-1508>
- [17] JADALIHA M, ZONG X, MALAKAR P, RAY T, SINGH DK et al. Functional and prognostic significance of long non-coding RNA MALAT1 as a metastasis driver in ER negative lymph node negative breast cancer. *Oncotarget* 2016; 7: 40418–40436. <https://doi.org/10.18632/oncotarget.9622>
- [18] GUTSCHNER T, HÄMMERLE M, EISSMANN M, HSU J, KIM Y et al. The noncoding RNA MALAT1 is a critical regulator of the metastasis phenotype of lung cancer cells. *Cancer Res* 2013; 73: 1180–1189. <https://doi.org/10.1158/0008-5472.CAN-12-2850>
- [19] WEI L, LI J, HAN Z, CHEN Z, ZHANG Q. Silencing of lncRNA MALAT1 Prevents Inflammatory Injury after Lung Transplant Ischemia-Reperfusion by Downregulation of IL-8 via p300. *Mol Ther Nucleic Acids* 2019; 18: 285–297. <https://doi.org/10.1016/j.omtn.2019.05.009>
- [20] HU L, WU Y, TAN D, MENG H, WANG K et al. Up-regulation of long noncoding RNA MALAT1 contributes to proliferation and metastasis in esophageal squamous cell carcinoma. *J Exp Clin Cancer Res* 2015; 34: 7. <https://doi.org/10.1186/s13046-015-0123-z>

- [21] XU Y, ZHANG X, HU X, ZHOU W, ZHANG P et al. The effects of lncRNA MALAT1 on proliferation, invasion and migration in colorectal cancer through regulating SOX9. *Mol Med* 2018; 24: 52. <https://doi.org/10.1186/s10020-018-0050-5>
- [22] DJEBALI S, DAVIS CA, MERKEL A, DOBIN A, LASS-MANN T et al. Landscape of transcription in human cells. *Nature* 2012; 489: 101–108. <https://doi.org/10.1038/nature11233>
- [23] JOHANSSON P, LIPOVICH L, GRANDÉR D, MORRIS KV. Evolutionary conservation of long non-coding RNAs; sequence, structure, function. *Biochim Biophys Acta* 2014; 1840: 1063–1071. <https://doi.org/10.1016/j.bbagen.2013.10.035>
- [24] WILUSZ JE, FREIER SM, SPECTOR DL. 3'-end processing of a long nuclear-retained noncoding RNA yields a tRNA-like cytoplasmic RNA. *Cell* 2008; 135: 919–932. <https://doi.org/10.1016/j.cell.2008.10.012>
- [25] BROWN JA, BULKLEY D, WANG J, VALENSTEIN ML, YARIO TA et al. Structural insights into the stabilization of MALAT1 noncoding RNA by a bipartite triple helix. *Nat Struct Mol Biol* 2014; 21: 633–640. <https://doi.org/10.1038/nsmb.2844>
- [26] BROWN JA, VALENSTEIN ML, YARIO TA, TYCOWSKI KT, STEITZ JA. Formation of triple-helical structures by the 3'-end sequences of MALAT1 and MEN $\beta$  noncoding RNAs. *Proc Natl Acad Sci U S A* 2012; 109: 19202–19207. <https://doi.org/10.1073/pnas.1217338109>
- [27] MESEURE D, VACHER S, LALLEMAND F, ALSIBAI KD, HATEM R et al. Prognostic value of a newly identified MALAT1 alternatively spliced transcript in breast cancer. *Br J Cancer* 2016; 114: 1395–1404. <https://doi.org/10.1038/bjc.2016.123>
- [28] AGEELI AA, MCGOVERN-GOOCH KR, KAMINSKA MM, BAIRD NJ. Finely tuned conformational dynamics regulate the protective function of the lncRNA MALAT1 triple helix. *Nucleic Acids Res* 2019; 47: 1468–1481. <https://doi.org/10.1093/nar/gky1171>
- [29] MCCARTHY A. Third generation DNA sequencing: pacific biosciences' single molecule real time technology. *Chem Biol* 2010; 17: 675–676. <https://doi.org/10.1016/j.chembiol.2010.07.004>
- [30] ABDEL-GHANY SE, HAMILTON M, JACOBI JL, NGAM P, DEVITT N et al. A survey of the sorghum transcriptome using single-molecule long reads. *Nat Commun* 2016; 7: 11706. <https://doi.org/10.1038/ncomms11706>
- [31] WANG B, TSENG E, REGULSKI M, CLARK TA, HON T et al. Unveiling the complexity of the maize transcriptome by single-molecule long-read sequencing. *Nat Commun* 2016; 7: 11708. <https://doi.org/10.1038/ncomms11708>
- [32] GAO S, REN Y, SUN Y, WU Z, RUAN J et al. PacBio full-length transcriptome profiling of insect mitochondrial gene expression. *RNA Biol* 2016; 13: 820–825. <https://doi.org/10.1080/15476286.2016.1197481>
- [33] AHMAD A, LIN H, SHATABDA S. Locate-R: Subcellular localization of long non-coding RNAs using nucleotide compositions. *Genomics* 2020; 112: 2583–2589. <https://doi.org/10.1016/j.ygeno.2020.02.011>
- [34] BELLUCCI M, AGOSTINI F, MASIN M, TARTAGLIA GG. Predicting protein associations with long noncoding RNAs. *Nat Methods* 2011; 8: 444–445. <https://doi.org/10.1038/nmeth.1611>
- [35] PAZ I, KOSTI I, ARES M JR, CLINE M, MANDEL-GUT-FREUND Y. RBPmap: a web server for mapping binding sites of RNA-binding proteins. *Nucleic Acids Res* 2014; 42: W361–367. <https://doi.org/10.1093/nar/gku406>
- [36] LIVAK KJ, SCHMITTGEN TD. Analysis of relative gene expression data using real-time quantitative PCR and the 2<sup>(-Delta Delta C(T))</sup> Method. *Methods* 2001; 25: 402–408. <https://doi.org/10.1006/meth.2001.1262>
- [37] SOARES RJ, MAGLIERI G, GUTSCHNER T, DIEDERICH S, LUND AH et al. Evaluation of fluorescence in situ hybridization techniques to study long non-coding RNA expression in cultured cells. *Nucleic Acids Res* 2018; 46: e4. <https://doi.org/10.1093/nar/gkx946>
- [38] NIWA J, YAMADA S, ISHIGAKI S, SONE J, TAKAHASHI M et al. Disulfide bond mediates aggregation, toxicity, and ubiquitylation of familial amyotrophic lateral sclerosis-linked mutant SOD1. *J Biol Chem* 2007; 282: 28087–28095. <https://doi.org/10.1074/jbc.M704465200>
- [39] LANG Y, KONG X, HE C, WANG F, LIU B et al. Musashi1 Promotes Non-Small Cell Lung Carcinoma Malignancy and Chemoresistance via Activating the Akt Signaling Pathway. *Cell Physiol Biochem* 2017; 44: 455–466. <https://doi.org/10.1159/000485012>
- [40] WILUSZ JE, FREIER SM, SPECTOR DL. 3' end processing of a long nuclear-retained noncoding RNA yields a tRNA-like cytoplasmic RNA. *Cell* 2008; 135: 919–932. <https://doi.org/10.1016/j.cell.2008.10.012>
- [41] WILUSZ JE, JNBAPTISTE CK, LU LY, KUHN CD, JOSHUA-TOR L et al. A triple helix stabilizes the 3' ends of long noncoding RNAs that lack poly(A) tails. *Genes Dev* 2012; 26: 2392–2407. <https://doi.org/10.1101/gad.204438.112>
- [42] SU K, WANG N, SHAO Q, LIU H, ZHAO B et al. The role of a ceRNA regulatory network based on lncRNA MALAT1 site in cancer progression. *Biomed Pharmacother* 2021; 137: 111389. <https://doi.org/10.1016/j.biopha.2021.111389>
- [43] LEUNG A. The Whereabouts of microRNA Actions: Cytoplasm and Beyond. *Trends Cell Biol* 2015; 25: 601–610. <https://doi.org/10.1016/j.tcb.2015.07.005>
- [44] WIEMER E. Prognostic Circulating MicroRNA Biomarkers in Early-Stage Non-Small Cell Lung Cancer: A Role for miR-150. *Clin Pharmacol Ther* 2018; 103: 968–970. <https://doi.org/10.1002/cpt.972>
- [45] DAI FQ, LI CR, FAN XQ, TAN L, WANG RT et al. miR-150-5p Inhibits Non-Small-Cell Lung Cancer Metastasis and Recurrence by Targeting HMGA2 and  $\beta$ -Catenin Signaling. *Mol Ther Nucleic Acids* 2019; 16: 675–685. <https://doi.org/10.1016/j.omtn.2019.04.017>
- [46] LIU X, SEMPERE LF, GALIMBERTI F, FREEMANTLE SJ, BLACK C et al. Uncovering growth-suppressive MicroRNAs in lung cancer. *Clin Cancer Res* 2009; 15: 1177–1183. <https://doi.org/10.1158/1078-0432.CCR-08-1355>

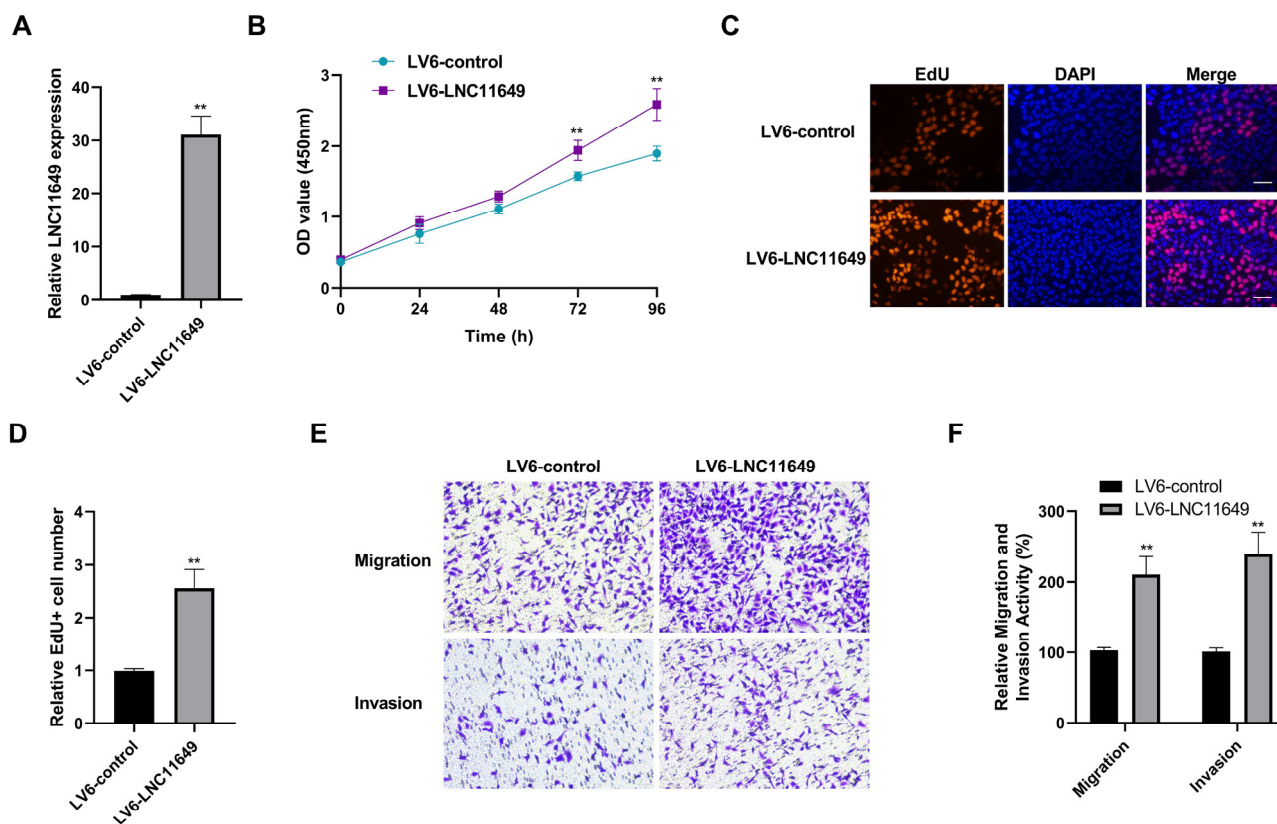
- [47] CAMPAYO M, NAVARRO A, VIÑOLAS N, DIAZ T, TEJERO R et al. Low miR-145 and high miR-367 are associated with unfavourable prognosis in resected nonsmall cell lung cancer. *Eur Respir J* 2013; 41: 1172–1178. <https://doi.org/10.1183/09031936.00048712>
- [48] FOROUZANFAR M, LACHINANI L, DORMIANI K, NASR-ESFAHANI MH, GURE AO et al. Intracellular functions of RNA-binding protein, Musashi1, in stem and cancer cells. *Stem Cell Res Ther* 2020; 11: 193. <https://doi.org/10.1186/s13287-020-01703-w>
- [49] BLEY N, HMEDAT A, MÜLLER S, ROLNIK R, RAUSCH A et al. Musashi-1-A Stemness RBP for Cancer Therapy. *Biology (Basel)* 2021; 10. <https://doi.org/10.3390/biology10050407>
- [50] KHARAS MG, LENGNER CJ. Stem Cells, Cancer, and MUSASHI in Blood and Guts. *Trends Cancer* 2017; 3: 347–356. <https://doi.org/10.1016/j.trecan.2017.03.007>
- [51] WANG XY, YU H, LINNOILA RI, LI L, LI D et al. Musashi1 as a potential therapeutic target and diagnostic marker for lung cancer. *Oncotarget* 2013; 4: 739–750. <https://doi.org/10.18632/oncotarget.1034>

[https://doi.org/10.4149/neo\\_2022\\_220705N689](https://doi.org/10.4149/neo_2022_220705N689)

## Functions of long non-coding RNA LNC11649 in non-small cell lung cancer cells as a reprocessed form of MALAT1

Jun-Zhe QI<sup>1</sup>, Ting-Ting ZHAO<sup>2</sup>, Shu-Shan QI<sup>2,\*</sup>

### Supplementary Information



Supplementary Figure S1. Functional analysis of LNC11649 in HCC827 cells. A) LNC11649 lentiviral vector was transfected into HCC827 cells for 48 h. The relative expression content of LNC11649 was measured by quantitative PCR. \*\* $p < 0.01$  B) Detection of cell activity at different time points by CCK-8 after transfection of LNC11649 expression plasmid or control plasmid (1  $\mu\text{g}/\text{well}$  in the 24-well plate) in HCC827 cells. \*\* $p < 0.01$  C, D) Detection of cell proliferation by EdU staining after transfection of LNC11649 expression plasmid or control plasmid in HCC827 cells for 24 h (Scale, 50  $\mu\text{m}$ ). Compared with LV6-control group, \*\* $p < 0.01$ . E, F) Detection of cell migration and invasion by transwell assay after transfection of LNC11649 expression plasmid or control plasmid in HCC827 cells for 24 h (Scale, 50  $\mu\text{m}$ ). Compared with LV6-control group, \*\* $p < 0.01$

Supplementary Tables S1–S4 are available in the online version for download.